Experimental Multipath Performance of Galileo CBOC per Environmental Context

Maximilian von Arnim[1,*,†], Damien Vivet[1,†] and Yoko Watanabe[1,†]

[1]Fédération ENAC ISAE-SUPAERO ONERA, Université de Toulouse, Toulouse, France

Abstract

The environmental context remains a key impact on Global Navigation Satellite System (GNSS) positioning solutions for modern mobile applications. Novel approaches seek to explicitly include a semantic context detector into the estimator to mitigate context-specific phenomena such as multipath effect, the primary environmental disturbance. The European GNSS Galileo was explicitly designed with greater resistance to multipath than legacy GPS signals. With the aim of developing context-adaptive estimation algorithms, this paper focuses on context-dependent multipath error modeling for Galileo E1B/C signals and its comparison with the models for GPS L1 C/A. We consider four distinct environmental contexts: urban canyons, open sky, tree-covered areas, and general urban settings. Compared to GPS L1 C/A, the multipath error is much reduced for Galileo E1B/C signals thanks to their Multiplexed Binary Offset Carrier (MBOC) modulation. The results show different behaviors between low-cost and high-precision receivers in the most complex urban context, suggesting the need to establish receiver-aware context-adaptation strategies for resilient GNSS-based navigation.

Keywords

Environmental context, Adaptive estimator, Multipath, Black-box receiver

1. Introduction

Challenges imposed by the environmental context of a GNSS user remain one of the key hurdles to ubiquitous positioning. The Global Positioning System (GPS) was originally developed with minimal concern for multipath effects, and only a minimum number of satellites to guarantee worldwide coverage. Later, modernized GPS and Galileo modulations were chosen specifically to improve this disturbance.

Support for multiple GNSS has become standard among recent commercial receivers. Virtually all devices receive GPS L1 signals, and are therefore compatible with Galileo E1. There are obvious benefits to be gained from more visible satellites alone. In addition, Galileo's MBOC-based modulation on E1 promises improved accuracy, on top of other Galileo-specific advantages.

Multipath effects on different modulations have been studied both theoretically and experimentally. Our work is based on [1], which presented joint Galileo/GPS multipath residuals after binning the data by C/N_0. Key theoretical results for various Binary Offset Carrier (BOC) modulations are given in [2]. Recent work has looked into ever-more-capable smartphone receivers [3].

This theoretical advantage comes at increased computational cost, however, and thus hardware cost [4]. Some of the advantages are only exploitable given greater frontend bandwidth [5, 6]. There is also an inherent ambiguity that adds complexity to the receiver algorithms [5]. A receiver implementation can choose among a plethora of methods that address these challenges. Conversely, users of such a "black box" device find themselves faced with the conundrum of modeling the random pseudorange noise to properly tune their estimators.

We previously found standard models for Binary Phase Shift Keying (BPSK) signals applicable to two receivers in a dataset [7]. This enabled the development of a model for the additional error expected in distinct environmental contexts, which was combined with a semantic context detector to create

WIPHAL'25: Work-in-Progress in Hardware and Software for Location Computation June 10–12, 2025, Rome, Italy

*Corresponding author.

†These authors contributed equally.

maximilian.von-arnim@isae-supaero.fr (M. v. Arnim); damien.vivet@isae-supaero.fr (D. Vivet); yoko.watanabe@onera.fr (Y. Watanabe)

context-adaptive estimators. It therefore becomes a need to establish a baseline for the performance of mass-market Galileo receivers, based on which we can extend our method to MBOC multipath effects.

The main contributions of this paper are:

- A discussion of state-of-the-art MBOC processing and their potential use in two commercial receivers given the observed Galileo E1 pseudorange errors.
- A context-dependent statistical error model caused by multipath on Galileo E1, in comparison to a prior study on GPS L1 using data obtained in Toulouse, France.
- Perspectives for a joint Galileo/GPS position, velocity and time (PVT) solution using semantic environmental context classifiers.

2. Methodology

Our prior work empirically modeled GPS L1 Coarse/Acquisition (C/A) pseudorange multipath depending on semantic context information [7]. These models improve the localization of applications using commercial black-box receivers in challenging environments. In this contribution, we extend the model to the Galileo E1B/C Open Service (O/S) signal. For brevity and because no other signals on these frequencies were included, we will refer to them simply as E1 and L1. The methodology remains unchanged.

A three-step process illustrated in Fig. 1a can isolate the multipath error from the pseudoranges observed by a black-box commercial receiver. To recapitulate, we use the standard pseudorange model [8] for receiver x and satellite i

$$P_x^i = R_x^i + b_x c - b^i c + h_x + h^i + A_x^i + M_x^i + \eta_x^i \tag{1}$$

where

P	pseudorange
R	true range
bc	clock bias $\times$ speed of light
h	hardware bias
A	atmospheric = ionospheric + tropospheric delay
M	multipath delay
η	random noise, ephemeris and other unmodeled errors

First, pseudoranges recorded by the receiver under test D yield range-free double-differences $\Delta\epsilon$ between satellites $i \neq j$ and a chosen pivot satellite j

$$\Delta\epsilon_{\mathrm{D,B}}^{i,j} = \Delta M_{\mathrm{D}}^{i,j} + \eta_{\mathrm{D,B}}^{i,j} \tag{2}$$

with the help of a local base station B and the ground truth position, a method developed by [9] and refined for our data [10]. The remaining term contains the receivers' random noise η and the multipath error caused by the local environment. In this case, the procedure yields not the absolute multipath M but the relative multipath ΔM between the pivot satellite and the i-th satellite. As carrier-phase measurements are not required, any black-box receiver can be studied in this manner. The mobile reference receiver R can serve as D as well.

Separately, the GNSS data is classified into four environmental contexts by a camera-aided context detection algorithm [11]: *Open Sky* (OS) in near-ideal conditions, *Trees* (TR) when under foliage, *Canyon* (CA) for constrained environments (frequently dubbed urban canyon) and *Urban* (UB) for generic urban environments. For illustration, the environment ground truth labeling heuristic is reproduced in Fig. 2. A Support Vector Machine (SVM) was trained on these labels and an input vector consisting of Galileo and GPS observables (C/N_0, Single Point Positioning (SPP) residuals, elevation, number of received satellites) labeled by the sky-facing camera as Line-of-Sight (LOS) or Non-Line-of-Sight (NLOS) at each epoch.

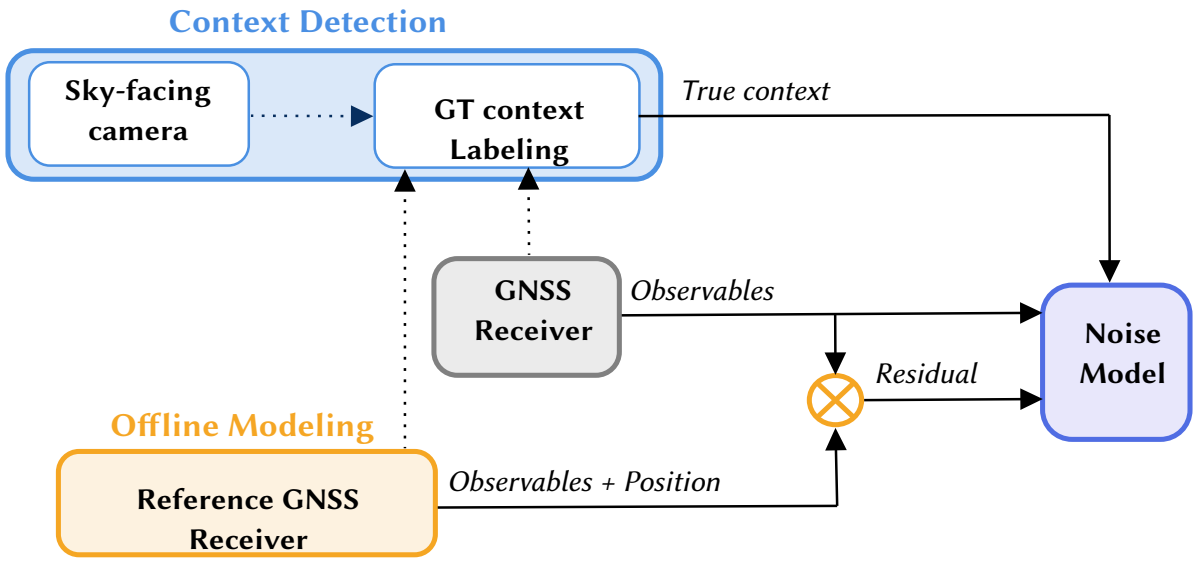

(a) Offline analysis of GNSS residuals for multipath error modeling

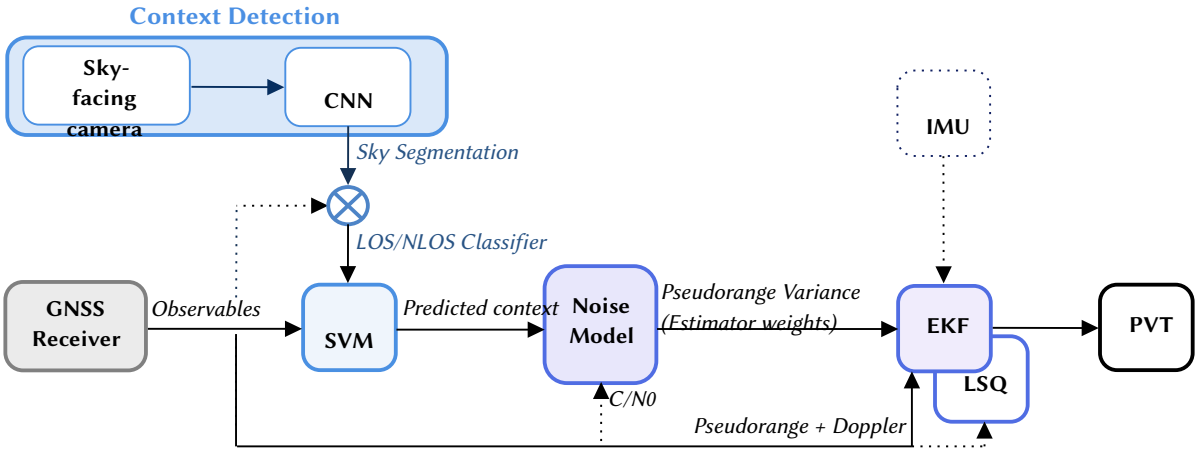

(b) Context-adaptive parametrization for the estimators' measurement model

Figure 1: Block diagrams for the two-step procedure

Finally, the statistical properties of $\Delta\epsilon$ are calculated for each context as a function of C/N_0, thus allowing us to fit the context-independent thermal noise model σ_{DLL} [12] and a context-adaptive SIGMA-ϵ multipath noise model [13]

$$Var(\Delta M) = \sigma_c^2 = C_c \cdot 10^{-\frac{(C/N_0)_{dB}}{10}} \tag{3}$$

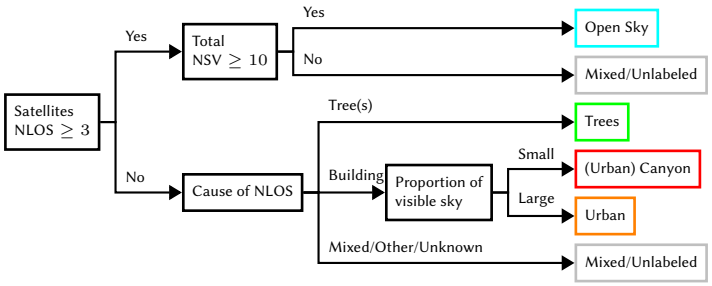

Figure 2: Context detection heuristic for the ground truth labels [11].

$$\left(\frac{\sigma_{DLL}}{cT_c}\right)^2 = \begin{cases} \frac{B_n}{2(c/n_0)} D\left[1+\frac{2}{T(c/n_0)(2-D)}\right], & DB_{fe}T_c \geq \pi \\ \frac{B_n}{2(c/n_0)}\left(\frac{1}{B_{fe}T_c}+\frac{B_{fe}T_c}{\pi-1}\left(D-\frac{1}{B_{fe}T_c}\right)^2\right)\left[1+\frac{2}{T(c/n_0)(2-D)}\right], & 1 < DB_{fe}T_c < \pi \\ \frac{B_n}{2(c/n_0)}\left(\frac{1}{B_{fe}T_c}\right)\left[1+\frac{1}{T(c/n_0)}\right], & DB_{fe}T_c \leq 1 \end{cases} \tag{4}$$

It is parameterized by $C_c \geq 0$ for each context $c \in \{OS, TR, CA, UB\}$. This is an empirical parameter without immediate physical meaning. The SIGMA-ε model is a function of C/N_0, not elevation or other parameters more directly linked to the environment. As seen in our results, the C/N_0 remains a more informative parameter concerning the presence and magnitude of multipath than the satellite elevation alone; other options like the use of NLOS classifiers have found success in prior work but depend on additional sensors [14] or a map [15] that we seek to avoid. We fit Eq. 3 to the data using nonlinear weighted least squares, where the weights are n^2 with n the number of samples obtained for each C/N_0. Samples with low $C/N_0 < 20\,\mathrm{dB\,Hz}$ are excluded from the fit due to poor reliability. The sample statistics are plotted as dashed lines in Fig. 3 while the fitted model is shown by solid lines.

The thermal noise model σ_{DLL} of the BPSK modulation of the GPS L1 C/A signal is well understood and applicable to both of our commercial receivers. A closed form equation [12] is given in Eq. 4 as a function of c/n_0 where $C/N_0 = 10\log_{10}(c/n_0)$. Observing that the double differences $\Delta\epsilon$ in open sky environments are nearly unbiased and Gaussian, we can suppose that this environment is nearly multipath-free. This permits us to choose parameters that let the theoretical model match each receiver's measurements even if the model has many degrees of freedom. We can set the bandwidth of the analog front end B_{fe}, the predetection integration time T, the chip spacing D and the Delay Lock Loop (DLL) bandwidth B_n. The chip length T_c in seconds is defined by the signal, convertible to meters with the speed of light c. We constrain their values to a certain expected range and make use of the rule-of-thumb 3σ tracking threshold [12] to determine suitable parameters.

Galileo's E1B/C MBOC modulation, however, adds more complexity and becomes more challenging to model. Its residuals were thus omitted in our prior work. A discussion of both the data and some black-box Composite Binary Offset Carrier (CBOC) receiver properties will be the focus of this contribution.

3. Dataset

The statistical analysis of the GNSS multipath errors is based on a public dataset constructed in our previous work [11]. Vision and GNSS data was collected on a car in and around Toulouse, in southern France; the multi-hour dataset comprises 116,765 GNSS samples (@5 Hz) from a commercial ublox M8T receiver and 46,589 images (@2 Hz) taken by a sky-facing fisheye camera. A PVT ground truth is included, making use of Novatel PwrPak7 carrier phase and Inertial Measurement Unit (IMU) measurements in post-processing by Novatel's Inertial Explorer software. This contribution will focus on the trajectory "Dataset_3" (recording started on 2022-03-24 14:32:41+01:00). The multipath analysis relies on additional unpublished data: the pseudoranges and C/N_0 recorded by the ground truth mobile and base station receivers. These can be provided upon request.

4. Results

After applying the method to our data, we can plot the standard deviation of the obtained double differences over C/N_0 in Fig. 3. This allows us to separate the internal noise of the receiver from the environmental effects to study each term individually.

Figure 3 shows the results obtained for the two receivers and for Galileo and GPS signals. The left Figs. 3a and 3c show the Novatel receiver data, while the right Figs. 3b and 3d show those for the ublox

receiver. The y-axis scale is different for the two receivers to improve visibility of the Novatel receiver's features. The two signals remain comparable within each receiver. The top Figs. 3a and 3b present Galileo E1 signals. For reference, we include the results previously obtained for GPS in Figs. 3c & 3d. NOTE TO EDITOR: WILL PROVIDE ZOOM OF HIGH C/N0 REGION LATER.

On each figure, the observed standard deviation of the error and its fitted model are shown in dashed and solid lines, respectively. The line colors represent the environmental context: *Open Sky* (OS; blue), *Trees* (TR; green), *Urban* (UB; orange) and *Canyon* (CA; red). The context-specific model parameter C_c is included in the legend.

The nominal thermal noise model σ_{DLL}, as fitted to the Open Sky (OS) context, remains parameterized by Table 1 assuming a non-coherent Early-minus-Late Power (EMLP) discriminator. For easier comparison, both signals were assigned the same parameters and the same model, customized only to the receiver. It is shown as a solid black line.

Concerning the context-dependent statistics, E1 generally shows less impact of the environment than L1. For both receivers and signals, the environment with the largest noise is *Urban* while the least noise is found in *Open Sky* contexts. We will commence by examining the Novatel receiver, then study the ublox receiver in greater detail.

The Novatel receiver produces much less noisy pseudoranges in all contexts. However, it is only able to track higher C/N_0 signals. Its tracking threshold for E1 is around $28\,\mathrm{dB\,Hz}$ while L1 can be tracked down to $24\,\mathrm{dB\,Hz}$. We note that the cutoff for E1 is higher in the *Trees* environment, and likewise for L1 in the *Open Sky* environment, though this may be an artifact of the dataset. There are few samples close to the tracking threshold. The maximum recorded C/N_0 is the same for both signals, around $52\,\mathrm{dB\,Hz}$.

The Novatel receiver shows no significant effect of the environmental context for strong signals above $43\,\mathrm{dB\,Hz}$ to $45\,\mathrm{dB\,Hz}$. We can assume that these are LOS signals with minimal multipath interference.

Below this threshold, differences in the environments become visible. All non-*Open Sky* contexts are much noisier than *Open Sky*, in some cases more than four times as much at the same received signal power.

Qualitatively, the data for both signals appears similar. *Urban* and *Canyon* environments are much noisier with both giving about the same results. The *Trees* context usually finds itself under those two, but above *Open Sky*. This in-between status is more pronounced on E1 signals. A clear correlation with C/N_0 is observed, similar in shape to the underlying receiver noise model given by Eq. 4.

Quantitatively, however, the E1 pseudoranges are much less noisy in all environments. The maximum standard deviation of E1 is capped at less than $6\,\mathrm{m}$ while L1 reaches more than $15\,\mathrm{m}$. In particular the *Open Sky* measurements become significantly more accurate than L1 for medium-strength observations under $40\,\mathrm{dB\,Hz}$, although the two signals remain similar at higher C/N_0.

The fitted SIGMA-ε model remains relatively close to the Novatel observations from $30\,\mathrm{dB\,Hz}$ to $45\,\mathrm{dB\,Hz}$. Deviations can be explained by the presence of rare outliers that have great impact on the statistical sample moments. This is particularly pronounced towards the tracking threshold, where we have few samples to begin with. Thanks to the E1 signal's better performance in lower C/N_0, the random noise model σ_{DLL} chosen for L1 is no longer a good fit to the *Open Sky* variance. Fortunately, the context-dependent error dominates in non-*Open Sky* environments. Under those conditions, the fit process for the SIGMA-ε model is relatively robust to errors in the random noise model.

Now, to the ublox. Its tracking threshold is similar for both signals, reaching down to less than $10\,\mathrm{dB\,Hz}$. The highest recorded signal strength is about $2\,\mathrm{dB}$ less for E1 than L1, at $49\,\mathrm{dB\,Hz}$ and $51\,\mathrm{dB\,Hz}$, respectively.

Like the Novatel receiver, both signals and all non-*Open Sky* environments perform similarly for $C/N_0 \geq 40\,\mathrm{dB\,Hz}$. The ublox also shares the behavior of the Novatel receiver that very strong L1 signals over $45\,\mathrm{dB\,Hz}$ are nearly context-independent. Another similarity between the two receivers is the reduced E1 error in *Open Sky* environments for weaker signals, visible in the ublox' case for $C/N_0 \leq 30\,\mathrm{dB\,Hz}$, while both signals are approximately equal when looking at higher-C/N_0 observations.

There are some differences between the two receivers. The most striking is the much increased noise both in the *Open Sky* baseline and in the other environments. Nonetheless, the E1 pseudoranges remain

Table 1
DLL parameters of σ_{DLL} (Eq. 4) as plotted in Fig. 3. B_{fe} and T_c are combined into one term as both signals share the same chip length, and the terms are not separable in Eq. 4.

	$B_{fe}T_c$	T	D	B_n
NovAtel PwrPak7	7 chip^{-1}	0.02 s	0.1 chip	0.2 Hz
ublox-M8T			1 chip	

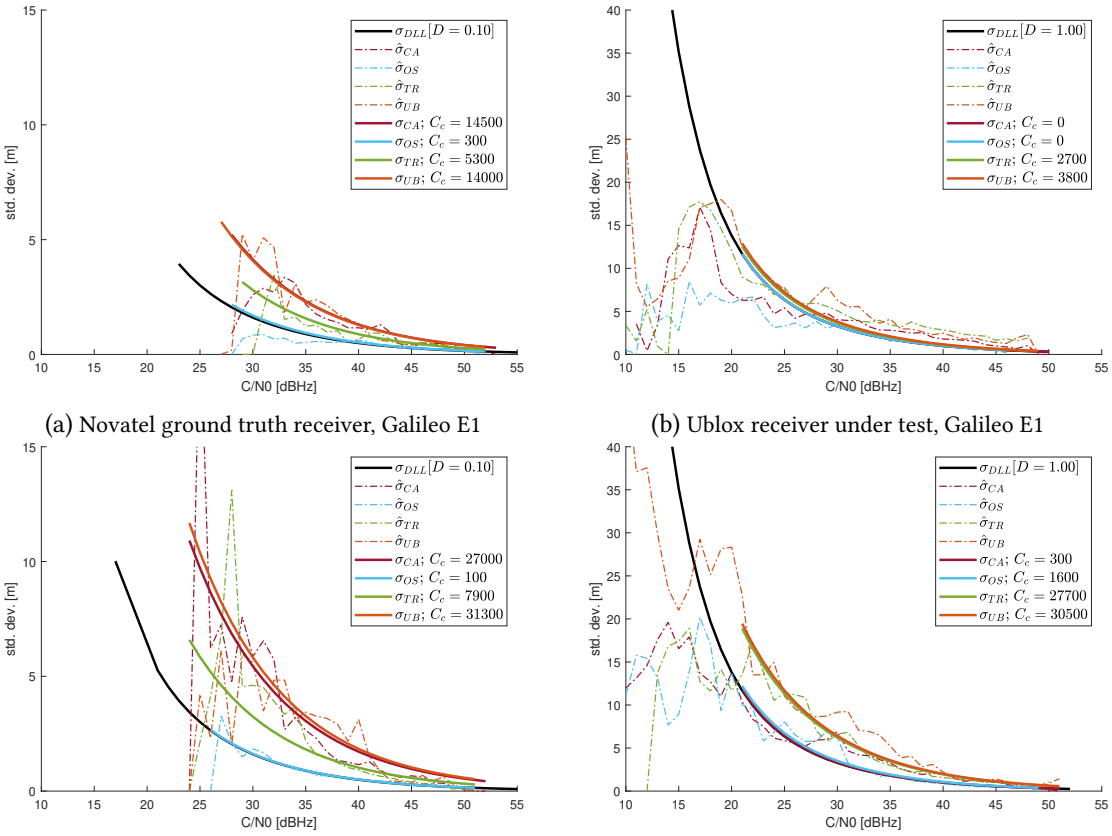

(a) Novatel ground truth receiver, Galileo E1

(b) Ublox receiver under test, Galileo E1

(c) Novatel ground truth receiver, GPS L1

(d) Ublox receiver under test, GPS L1

Figure 3: Empirical ($\hat{\sigma}$), DLL (σ_{DLL}) and fitted model (σ_c) standard deviation of the residual $\Delta\epsilon$ versus C/N_0 per context

significantly less noisy than their L1 counterparts for weaker $C/N_0 \leq 30\,\text{dB Hz}$. Stronger E1 signals appear to be subject to a constant added pseudorange variance that is not discernible in the L1 data. All non-*Open Sky* environments produce similar sample variances of ublox E1 pseudoranges while there remains a clear separation of its L1 results in each environment. As a general observation, the *Urban* environment experiences the greatest additional L1 error, followed by the *Trees* and finally the *Canyon* environments.

This is reflected by the different fit parameters. We note, though, that the fit parameters of ublox E1 signals are perhaps less representative of the actual environmental effects, since the fit remains based on additional noise to the L1 random noise model, a model which is clearly not applicable for the entire C/N_0 range. Unlike the Novatel receiver, the random noise of the ublox receiver appears to dominate over the environment-specific effects, so this modeling error becomes relevant. The context-adaptive SIGMA-ε model Eq. 3 previously proposed for L1 pseudoranges would still be a reasonable choice to model the context-dependent noise on E1 observations if we were able to better characterize the context-independent thermal noise σ_{DLL} on E1 pseudoranges across the entire C/N_0 range.

5. Discussion

Given the observation that Galileo E1 pseudoranges are less noisy and less sensitive to specific environmental contexts, it is worth a look into possible reasons why, as well as some explanations why other aspects are similar to GPS. This paves the way towards different context adaptation strategies for joint Galileo/GPS PVT estimation.

5.1. Thermal Noise

We observed in our results that the GPS/BPSK thermal noise model fits a limited C/N_0-range of Galileo signals on our two receivers. The following will summarize the theoretical models of optimal and suboptimal MBOC receivers. It will be shown that modeling a black-box BOC receiver is far from straightforward, thus justifying our choice to replace it with the BPSK model as the second-best alternative.

The general expression for the random noise of the Dot Product (DP), as well as the noncoherent and coherent EMLP discriminators is given by [6] and is applicable to all Galileo signals.

$$\left(\frac{\sigma_{DLL}}{cT_c}\right)^2 = \frac{B_n(1-0.5B_nT)}{(2\pi)^2(c/n_0)I_2^2}\left[I_1 + \frac{I_3^2 - |I_4|^2}{4T(c/n_0)I_5^2}\right] \tag{5}$$

where c, T_c, B_n, B_{fe}, D and T are the same as for Eq. 4. It is based on the generic integral terms

$$I_1 = \int_{-B_{fe}/2}^{B_{fe}/2} S_s(f)\sin^2(\pi f D T_c)\,df \tag{6}$$

$$I_2 = \int_{-B_{fe}/2}^{B_{fe}/2} f S_n(f)\sin(\pi f D T_c)\,df \tag{7}$$

$$I_3 = \int_{-B_{fe}/2}^{B_{fe}/2} S_s(f)df \tag{8}$$

$$I_4 = \int_{-B_{fe}/2}^{B_{fe}/2} S_s(f)e^{j2\pi f D T_c}df \tag{9}$$

$$I_5 = \int_{-B_{fe}/2}^{B_{fe}/2} S_n(f)\cos(\pi f D T_c)\,df \tag{10}$$

using normalized (unit power) Power Spectral Densities (PSDs) $S_s(f)$ and $S_n(f)$ for the signal and noise components, respectively, as a function of the frequency f and depending on the incoming modulation as well as the local replica. In the most generic case, these are

$$S_s(f) = \frac{|H_{tx}(f)H_{rx}(f)^*|\,|H(f)|^2}{\int_{-\infty}^{\infty}|H_{tx}(f)H_{rx}(f)^*|\,|H(f)|^2\,df} \tag{11}$$

$$S_n(f) = \frac{|H_{rx}(f)|^2\,|H(f)|^2}{\int_{-\infty}^{\infty}|H_{rx}(f)|^2\,|H(f)|^2\,df} \tag{12}$$

The complex transfer functions $H_{tx/rx}(f)$ describe the signal itself and its local replica while $H(f)$ describes the analog frontend. This latter term can be omitted if assuming an ideal band pass filter of bandwidth B_{fe}. Note that the local replica need not be a perfect replica. Some options including the transfer functions are given by [6].

A closed form solution exists for GPS' L1 C/A BPSK modulation (and is given in Eq. 4, approximating only the usually neglectable factor $(1-0.5B_nT)\approx 1$), but not for most other GNSS signals including those broadcast by Galileo.

The model given in Eq. 5 must therefore be evaluated numerically. As shown by [6], the performance of a chosen chain of reception is defined by the same parameters for BOC as for BPSK. An additional

variable of CBOC signals is the choice of the local replica. Further, Galieo's data-less pilot channel E1C and its MBOC implentation of CBOC adds another degree of freedom in the receiver design.

Unfortunately, the effect of each parameter is more challenging to see without a closed form, impairing our ability to manually select appropriate values. Worse, attempts to numerically fit Eq. 5 to the Galileo E1 *Open Sky* double-difference variances prove unfeasible due to the high number of degrees of freedom, the constraints on some parameters imposed by the signal and hardware properties and the need for recomputation of several of the integrals Eqs. 6-12 whenever a parameter is changed.

Unable to apply model Eq. 5 to our data with satisfactory results, we will instead review some literature on MBOC receivers and how that theory compares to our data. This may permit future work to choose a more suitable thermal noise model for a given black-box receiver.

Theoretically, BOC and especially MBOC offers significantly greater accuracy. BOC alone provides a much sharper autocorrelation peak, which yields performance gains worth at least $2\,\mathrm{dB}$ in C/N_0 [5] with MBOC adding the the equivalent of another $3\,\mathrm{dB}$ [16]. We see this effect in action for weaker *Open Sky* measurements, where E1 significantly outperforms L1. However, a real receiver rarely exploits the signal's full potential, which lay explain the similar *Open Sky* performance of high-C/N_0 L1 (BPSK) and E1 (MBOC) residuals on both receivers, though more pronounced on the low-cost ublox receiver.

First of all, the frontend bandwidth fundamentally constrains the digital backend's performance. A narrow frontend filter reduces the sharpness of the autocorrelation function. The frontend is shared for all signals but there is still a signal-specific aspect as each modulation comes with its own PSD [17].

In practice, the backend implementation of an MBOC receiver is far less straightforward than a BPSK receiver. Galileo implements MBOC using $\mathrm{CBOC}(6,1,1/11,+)$ for the data (E1B) and $\mathrm{CBOC}(6,1,1/11,-)$ for the pilot (E1C) channel, with the combined E1B/C power split equally between both.

Pilot and data channels can be processed separately or jointly. It is also possible to only track one or the other. The joint MBOC signal leads to a time-multiplexed signal of either only BOC(1,1) or only BOC(6,1), depending on the pseudo-random spreading codes of each channel, as illustrated in [18]. As discussed in [18, 19, 20], optimal MBOC tracking requires a receiver to track both channels. In naive implementations, this comes with significant processing overhead that can be reduced by the joint tracking proposed by [18]. Unfortunately, the receivers used in this dataset are too old to make use of such recent joint tracking research.

We observe a lower maximum C/N_0 measured for E1 than for L1 in the ublox receiver. The offset of about $2\,\mathrm{dB}$ is consistent with a receiver that would only track one of the two channels (most likely E1B due to the need for ephemeris data), given the nominal $1.5\,\mathrm{dB}$ difference between the individual E1 channels and L1 (C/A) [21, 22]. An ideal receiver should be able to measure accurate code delays despite this lower signal power by exploiting the much greater slope of BOC discriminators at the prompt replica compared to BPSK [20] but this is impacted by the frontend bandwidth. It is possible that our receivers only track E1B, especially the computationally more constrained ublox receiver.

Further, tracking either the full MBOC or either of the two CBOC signals with a perfect local replica adds computational cost. One of the earliest proposed methods was to time multiplex the replica [16] but it has become apparent that a simple $BOC(1,1)$ replica can track both MBOC and CBOC acceptably at reduced computational cost [6]. This option may have been chosen by our receivers' manufacturers.

A key issue for all BOC-based modulations is the appearance of secondary correlator peaks. They generally require narrower chip spacing than BPSK signals, with even values such as $D = 0.2$ being far from the theoretically obtainable optimum [20].

Simultaneously, narrow spacing raises the tracking C/N_0 threshold. The threshold depends on the thermal noise, the width and slope of the linear region of the discriminator's S-curve and the dynamic tracking stress [20]. The ability of the ublox M8T receiver to track E1 signals down to very low C/N_0 suggests a traditional wide spacing that BOC, in theory, does not permit. Instead, an option the ublox receiver may be employing is a BPSK-like method [23] that transforms the BOC autocorrelation function into a more BPSK-like unambiguous shape. This loses some of the BOC performance benefits but removes the secondary correlator peaks and allows the use of wider chip spacing.

To summarize, it remains much more challenging to model an MBOC receiver without access to its

inner workings. No single design choice would explain the observed pseudorange noise over the full C/N_0 range. Future work could record baseband or intermediate frequency samples for processing in a software receiver with full control over all parameters, but users of commercial black-box products may still find this discussion useful when evaluating or designing their navigation solution.

5.2. Multipath and Environmental Contexts

Having established the thermal noise and some probable choices for the receiver architecture, the multipath effects can be discussed with an eye on environmental contexts.

First of all, we note that compared to our previous work [7], the modified fit weights cause the fitted curves to approach each other in the Trees and Urban contexts for ublox data, and in the Canyon and Urban contexts for Novatel data. This corresponds to the intuition that an Urban context contains properties of both contexts. Their relevance depends on the receiver implementation.

The susceptibility to far multipath is reduced compared to BPSK in all of the BOC processing techniques [20, 6, 24] even if the full potential of MBOC is not exploited. If such a discriminator was implemented in the commercial devices used, it would explain the significantly improved performance in the Urban context. While we cannot determine the distance to the reflecting surface with our method, the more open structure of Urban environments would admit more far multipath than the more constrained Canyon.

We will note that a narrow chip spacing already has a similar, though weaker, effect [25]. The similar statistics of Urban and Canyon environments specifically for the Novatel receiver in each signal, respectively, are likely related to this. The ublox receiver, on the other hand, can exploit the E1 signal in Urban and Trees contexts in a manner that is not possible with BPSK on its low-cost hardware.

Of course, the gold standard would be a comparison with a software receiver using 2-bit baseband or intermediate frequency samples. As this is not provided in our dataset, such work is a promising avenue for future contributions.

5.3. Outlook on Context-Adaptive Navigation

The goal of our work remains context-aware navigation. Many applications in robotics and automation cannot develop their own receiver but rely on commercial products. We have shown that Galileo E1 pseudoranges of two black-box receivers are relatively insensitive to context changes, which makes them an ideal addition to estimators in challenging contexts such as urban areas. Our prior contribution [7] proposed the use of individual context adaptation parameters for each of the four classifiers: *Open Sky*, *Trees*, *Urban* and *Canyon*. The observed performance of Galileo could reduce the complexity of this approach. Instead, a simple distinction between *Open Sky* and non-*Open Sky* suffices.

The detection of non-*Open Sky* is much easier for a GNSS-only classification algorithm than distinguishing the more specific contexts, which require help from a sky-facing camera [11]. A Galileo-focused estimator can omit the camera for the purpose of context detection, even if cameras remain a highly useful tool for other tasks of autonomous systems.

In practice, most systems will (and should) employ all available constellations to maximize the available data. Our prior study on GPS L1 [7] noted challenges for IMU calibration when employing tightly-coupled estimators in Canyon contexts, caused by poor observability due to few visible satellites. More received satellites not only accelerate the filter convergence but also delay the critical point where bias estimation starts to fail. The estimator we discussed there, which adapts the state variables to the environmental context, can therefore be fine-tuned to the constellations available to the receiver.

A promising side-effect exists for more broad filter and sensor adaptation, as well as for the path planning aspect of navigation. Beyond the pure number of satellites visible (NSV), a combined GPS/Galileo system can venture further into Urban and Canyon environments than a pure GPS system without violating a certain accuracy requirement. The activation of power-hungry non-GNSS sensors, for example cameras, can be delayed. A path planning algorithm can choose to traverse a known

Figure 4: Image taken by the sky-facing fisheye camera used for NLOS and context classification

challenging area rather than take a detour, for example through downtown Toulouse, if both systems are available before a certain decision point.

Nonetheless, Galileo signals remain subject to NLOS, and even GNSS denial can never be ruled out. In one instance in the trajectory "Dataset_2", the Novatel receiver recorded a constant $45\,\mathrm{m}$ bias on one satellite while the vehicle waited at a traffic light. The local environment was captured by the fisheye camera, shown in Fig. 4, and classified as Urban; the red building on the right blocked the satellite's LOS. Such occurrences in Urban and Canyon contexts will need to be handled by robust estimators or additional sensors. Especially in Urban contexts, a joint Galileo/GPS system allows the user to exclude low-C/N_0 GPS or NLOS satellites without dropping under the minimum NSV. In Canyon contexts, a vision-based approach appears promising.

6. Conclusion

We studied the nominal variance of pseudorange errors due to multipath for two Global Navigation Satellite System (GNSS), Global Positioning System (GPS) and Galileo, to develop a context-specific model in four distinct environmental contexts: *Open Sky*, *Trees*, *Urban* and *Canyon*. The previously developed models for GPS L1 signals show a good fit to Galileo E1 signals in some circumstances, albeit with different parameters in line with the improved performance observed for Galileo. This model was obtained as a function of C/N_0 by the same method as for GPS, using a high-precision reference receiver and context ground truth labels to classify pseudorange residuals. A second low-cost receiver served as the primary device under test. The ground truth receiver's pseudoranges were also studied.

A literature study provided several models for the variance expected for receivers of Galileo's Multiplexed Binary Offset Carrier (MBOC) modulation. Critically, some of the features of MBOC force manufacturers to make tradeoffs between the theoretical accuracy, robustness and cost. These tradeoffs have greater impact than for legacy GPS signals and make it challenging to model a black-box receiver.

The similarity of both signals' performance, especially in high-C/N_0 *Open Sky* conditions, suggests that both manufacturers chose a suboptimal MBOC receiver implementation. Despite this tradeoff, Galileo E1 pseudoranges of both receivers exhibit much reduced impact by the environmental context than GPS L1. This shows how context-aware results obtained using a single GNSS constellation can be transferred to different systems after minor adaptation.

While the multipath-causing environment still has an effect, an application using a commercial Galileo receiver may be able to use a simpler context detection system. It can help calibrate other fused sensors that a context-adaptive system needs to traverse Canyons and similar contexts with high risk of GNSS denial, and it can mitigate outliers that are expected in Urban environments. The proposed parameter identification and adaptation strategy demonstrates the value inherent in context-adaptive estimation.

Acknowledgments

This work was supported by the Defense Innovation Agency (AID) of the French Ministry of Defense (research project CONCORDE N° 2019 65 0090004707501).

Declaration on Generative AI

The author(s) have not employed any Generative AI tools.

References

[1] E. R. Matera, A. J. Garcia-Peña, O. Julien, C. Milner, B. Ekambi, Characterization of Line-of-sight and Non-line-of-sight Pseudorange Multipath Errors in Urban Environment for GPS and Galileo, in: Proceedings of the 2019 International Technical Meeting of The Institute of Navigation, 2019, pp. 177–196. URL: https://enac.hal.science/hal-02138301.

[2] M. Irsigler, Multipath Propagation, Mitigation and Monitoring in the Light of Galileo and the Modernized GPS, Ph.D. thesis, Universität der Bundeswehr München, Munich, Germany, 2008.

[3] B. Bahadur, S. Schön, Improving the stochastic model for code pseudorange observations from Android smartphones, GPS Solutions 28 (2024).

[4] F. van Diggelen, High-Sensitivity GNSS, in: Y. T. J. Morton, F. van Diggelen, J. J. Spilker Jr., B. W. Parkinson (Eds.), Position, navigation, and timing technologies in the 21st century, Wiley and IEEE Press, 2021, pp. 445–479.

[5] O. Julien, G. Lachapelle, M. E. Cannon, Galileo L1 Civil Receiver Tracking Loops' Architecture, in: 2007 IEEE International Symposium on Circuits and Systems, IEEE Service Center, 2007, pp. 1737–1741.

[6] E. S. Lohan, Analytical performance of CBOC-modulated Galileo E1 signal using sine BOC(1,1) receiver for mass-market applications, in: IEEE/ION Position, Location and Navigation Symposium (PLANS 2010) ; Indian Wells, California, USA, 4 - 6 May 2010, IEEE, 2010, pp. 245–253.

[7] M. von Arnim, D. Vivet, Y. Watanabe, Context-adaptive GNSS and GNSS/INS estimation strategies based on prior statistical multipath knowledge., in: IEEE/ION Position, Location and Navigation Symposium (PLANS 2025) ; Salt Lake City, Utah, USA, April 28-May 1, 2025, 2025.

[8] D. Odijk, Positioning Model: Chapter 21, in: P. J. G. Teunissen, O. Montenbruck (Eds.), Springer handbook of global navigation satellite systems, Springer Handbooks Ser, Springer, 2017, pp. 605–638.

[9] E. R. Matera, A. J. Garcia-Peña, O. Julien, B. Ekambi, Characterization Of Pseudo-Range Multipath Errors In An Urban Environment, in: International Technical Symposium on Navigation and Timing 2018, 2018. URL: https://enac.hal.science/hal-01890371.

[10] M. von Arnim, D. Vivet, Y. Watanabe, Quantifying the GNSS Multipath Statistics by signal properties in urban, suburban and rural environments, Unpublished (2025).

[11] F. Feriol, Y. Watanabe, D. Vivet, Vision-enhanced GNSS-based environmental context detection for autonomous vehicle navigation, in: 2022 IEEE International Conference on Multisensor Fusion and Integration for Intelligent Systems (MFI), IEEE, 2022, pp. 1–6.
[12] P. W. Ward, GNSS Receivers: Chapter 8, in: E. D. Kaplan, C. J. Hegarty (Eds.), Understanding GPS/GNSS, GNSS Technology and Applications Series, Artech House, 2017, pp. 339–548.
[13] H. Hartinger, F. K. Brunner, Variances of GPS Phase Observations: The SIGMA-ε Model, GPS Solutions 2 (1999) 35–43.
[14] J.-i. Meguro, T. Murata, J.-i. Takiguchi, Y. Amano, T. Hashizume, GPS Multipath Mitigation for Urban Area Using Omnidirectional Infrared Camera, IEEE Transactions on Intelligent Transportation Systems 10 (2009) 22–30.
[15] F. Ruwisch, S. Schön, GNSS Feature Map: Representation of Signal Propagation-related Features in Urban Trenches, in: Proceedings of the 2022 International Technical Meeting of The Institute of Navigation, The International Technical Meeting of the The Institute of Navigation, The Institute of Navigation, 2022, pp. 701–711.
[16] J. Á. Á. Rodríguez, S. Wallner, G. W. Hein, E. Rebeyrol, O. Julien, C. Macabiau, L. Ries, A. de Latour, L. Lestarquit, J.-L. Issler, CBOC : an implementation of MBOC, in: CNES-ESA, 1st Workshop on GALILEO Signals and Signal Processing, 2006. URL: https://enac.hal.science/hal-01021795/.
[17] O. Julien, Design of Galileo L1F Receiver Tracking Loops: UCGE Reports Number 20227, Ph.D. thesis, University of Calgary, Calgary, AB, Canada, 2005.
[18] J. R. van der Merwe, F. Garzia, A. Rugamer, M. Saad, M. Overbeck, W. Felber, Efficient tracking of joint Galileo OS data and pilot components, in: 2020 European Navigation Conference (ENC), IEEE, 2020, pp. 1–10.
[19] B. A. Siddiqui, J. Zhang, M. Z. H. Bhuiyan, E. S. Lohan, Joint Data-Pilot acquisition and tracking of Galileo E1 Open Service signal, in: 2010 Ubiquitous Positioning Indoor Navigation and Location Based Service (UPINLBS), IEEE Service Center, 2010.
[20] A. Jovanovic, C. Mongrédien, Y. Tawk, C. Botteron, P.-A. Farine, Two-Step Galileo E1 CBOC Tracking Algorithm: When Reliability and Robustness Are Keys!, International Journal of Navigation and Observation 2012 (2012) 1–14.
[21] Galileo Open Service Signal-in-Space Interface Control Document: OS SIS ICD: Issue 2.1, 2023.
[22] A. Flores, NAVSTAR GPS Space Segment/Navigation User Interfaces: IS-GPS-200: Rev. M, El Segundo, CA, USA, 2021-04-13.
[23] A. Burian, E. Lohan, M. Renfors, BPSK-like Methods for Hybrid-Search Acquisition of Galileo Signals, in: 2006 IEEE International Conference on Communications, IEEE, 2006, pp. 5211–5216.
[24] A. Burian, Reduced-Complexity Code Synchronization in Multipath Channels for BOC Modulated CDMA Signals with Applications in Galileo and Modernized GPS Systems: Julkaisu 831 - Publication 831, Ph.D. thesis, Tampereen teknillinen yliopisto - Tampere University of Technology, Tampere, Finland, 2009.
[25] A. J. van Dierendonck, P. Fenton, T. Ford, Theory and Performance of Narrow Correlator Spacing in a GPS Receiver, NAVIGATION 39 (1992) 265–283.